Proceedings of the 10th International Conference on Asian and Pacific Coasts (APAC 2019) Hanoi, Vietnam, September 25-28, 2019

APPLICABILITY OF AN IMAGE-BASED ESTIMATION METHOD OF NEARSHORE MORPHOLOGY USING SMALL UNMANNED AERIAL VEHICLE

M. Yuhi[1], S. Ishida [2] and T. Saitoh [3]

ABSTRACT: Systematic monitoring of nearshore area provides useful information on sandy beaches over a wide range of temporal and spatial scales. In this study, accordingly, a simple local remote sensing system is developed to monitor the morphological variations of sandy beaches. This monitoring system consists of acquisition of geo-referenced video image of nearshore area from a small UAV (Unmanned Aerial Vehicle) and subsequent image analysis. Owing to the rapid development of information technology, high resolution photographic images of sea surface can be easily recorded at favorable location in a cost-efficient way. The subsequent quantification of morphological changes is carried out based on bright intensity patterns. First, the video images are converted to successive snapshots and rectified. After removing the small oscillations through semi-automatic identification of Ground Control Points (GCPs), the time-stack images of bright intensity variations are constructed for a series of cross-shore sections located at specified alongshore intervals. For each cross-section, the crest lines of waves are tracked out by inspecting the location of steep gradient in bright intensity variations. The local tracking results provide the celerity of waves. Combined with the observed wave period, the local water depth is estimated based on the linear dispersion relation. The system has been applied to the field observation of Uchinada Coast, Ishikawa, Japan facing to the Sea of Japan. The accuracy of geo-referencing was shown to be as small as a couple of pixels. The accuracy of morphological estimation based on image processing has been confirmed through comparison with a field survey using a jet bike. The image-based estimation results qualitatively reproduced the patterns of morphological variation. The typical error was in the range 0.2 to 0.8 m. These results demonstrated the capability of the developed system to remotely estimate the coastal morphology on sandy beaches.

Keywords: Unmanned Aerial Vehicle, local remote sensing, image analysis, nearshore morphology

INTRODUCTION

Beach behaviors often indicate complicated variabilities over a wide range of temporal and spatial scales under various environmental conditions. In order to obtain physical understanding on the underlying morphological processes, systematic monitoring of nearshore area as well as the development of effective monitoring tools are crucially important. For this purpose, image-based analysis system from a stationary monitoring platform have been developed and widely used in the last decades over the world (e.g., Holman and Stanley 2007; Holman and Haller 2012). More recently, rapid progress of Unmanned Aerial Vehicles (UAV) technology has been offering an alternative platform to acquire high-resolution remote-sensing data (e.g. Holman et al. 2017; Sun et al. 2019). The UAV system has the potential to provide an attractive measure for flexible field observations with high spatial and temporal resolution in a cost-efficient way.

The application of UAV in the monitoring of coastal morphological environments can be classified into two categories based on the area of measurements. One type of such studies is the photogrammetric survey of the topographies on coastal land area. Kuroiwa et al. (2016) analyzed the topography of foreshore and backshore of Uradome Beach, Japan by applying the Structure from Motion (SfM) technique to the aerial images observed from a small UAV. Turner et al. (2016) provided a review on the recent advances of UAV monitoring techniques for coastal surveying. The other type is related to the image-based estimation of underwater bathymetry in the surf zone. Matsuba and Sato (2018) conducted UAV-based monitoring of nearshore bathymetry on three beaches of different characteristics in Japan. A technique was shown to estimate nearshore bathymetry by extracting wave crest lines from pictures taken from a UAV. Holman et al. (2017) discussed the technical issues and procedures of surf zone monitoring using a small quadcopter and demonstrated their high potential for the monitoring of nearshore bathymetry. Su et al. (2019) developed an image-based nearshore bathymetry measurement method combined with a particle image velocimetry technique.

[1] School of Geoscience and Civil Engineering, Kanazawa University, Kakuma-Machi, Kanazawa City, 920-1192, JAPAN
[2] West Nippon Expressway Company Limited, 18F, Doujima Avanza, 1-6-10, Doujima, Kita-Ku, Osaka, 530-0003, JAPAN
[3] School of Geoscience and Civil Engineering, Kanazawa University, Kakuma-Machi, Kanazawa City, 920-1192, JAPAN

N. Trung Viet et al. (eds.), *APAC 2019,*
https://doi.org/10.1007/978-981-15-0291-0_75

Since the advance of UAV technology is very rapid, continuous and additional efforts are desired to further extend the applicability of UAV-based monitoring system.

In this study, accordingly, a local remote sensing system is developed in order to monitor morphological variations of sandy beaches with suitable resolution and high operational flexibility at low cost. The monitoring system consists of acquisition of geo-referenced video image of nearshore area from a small UAV and subsequent image analysis. After the semi-automatic corrections are completed for the small fluctuation induced by UAV drifts during flights, the propagation of wave crest is tracked based on the successive bright intensity images to estimate the local wave celerity. Referring to the dispersion relation of Airy's wave theory, the local depth of water is then estimated. The repeated use of this procedure provides the spatial distribution of water depth. The system is applied to the field observation of Uchinada Coast, Ishikawa, Japan facing to the Sea of Japan. First, the stability of the UAV positioning and the accuracy of geo-referencing is inspected. Then the accuracy of morphological estimation based on image processing has been confirmed through comparison with a field survey using a jet bike.

Field site

Uchinada Coast is a long sandy beach located on the middle north coast of Japan on the Sea of Japan (Fig.1(a)). The coast is considered to be a part of large-sacle littoral cell stretching approximately 75 km along the Sea of Japan coast. Figure 1(b) is a photograph of the Uchinada Coast and Kanazawa Port. The orientation of coastline is generally in NE-SW direction. Evolutions of beach cusps, large cusps, and crescent sandbars are often recognized. According to the morphodynamic classification by Wright and Short (1984), the field site is in the intermediate stage with rhythmic bar and beach.

Because the study area is micro tidal with a maximum tidal range of approximately 0.4 m, the sediment transport near the shoreline is mainly affected by seasonal wave actions.The seasonal variability in wave characteristics is significant, which is known as a typical feature observed at the Sea of Japan. The height and direction of incoming waves have been measured at Kanazawa Port that is adjacent to the study area. The wave characteristics have been recorded by the NOWPHAS (Nationwide Ocean Wave information network for Ports and HArborS) measurement system operated by the Ministry of Land, Infrastructure, Transport and Tourism, Japan (Nagai et al., 1994). The measurements have been conducted at approximately 15 m water depth located around 1,500 m offshore. Nguyen et al., (2015) has analyzed the NOWHPAS records from 1995 to 2010, and summarized the characteristics of the incoming waves as follows: Waves in summer are very calm, with their significant wave height mostly less than 1 m. The corresponding direction of incoming wave in summer is from the NNW, although the spreading of wave direction is relatively wide. On the contrary, high waves induced by strong East Asian winter monsoon often attack the coast in the winter. Waves with significant wave height exceeding 1m have often been recorded. The dominant direction of incoming waves in winter is from the NW to the NNW. Annual maximum significant wave height off the beach reaches 5 to 8 m. In spring and autumn, the wave heights are the medium. The dominant direction of annual longshore sediment transport near the shoreline is considered to be from the NE to the SW. At the south end of the area, the southwestward longshore sediment transport has been interrupted by the eastern groin of the Kanazawa Port (Fig. 1(b)). Combined with the sheltering effect of the main breakwater of Kanazawa Port (stretching out to approximately 13 m water depth with total length of 3.2 km), this has resulted in a local but rapid advancement of shoreline. The typical size of the sediment is generally in the range of fine sand at the study area. The median diameter of sediment is in the range 0.2 to 0.6 mm.

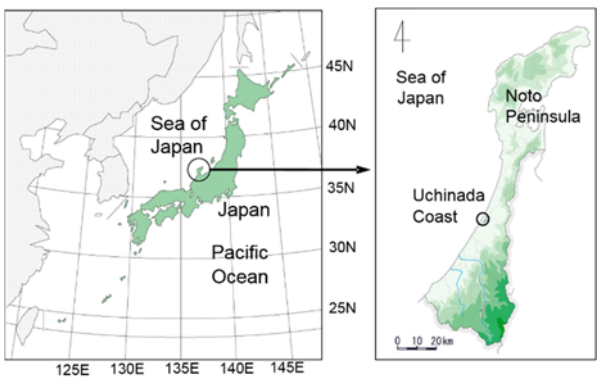

(a) Location of Uchinada Coast

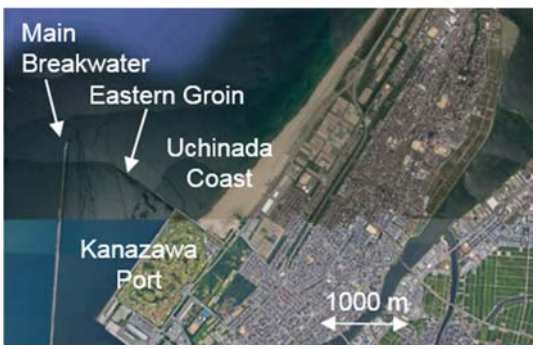

(b) Uchinada Coast and Kanazawa Port (adapted from Google Earth)

Fig. 1 Description of study area

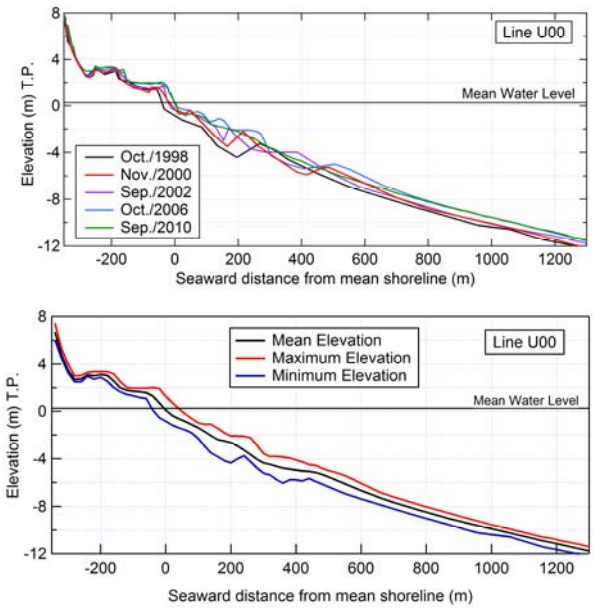

Fig. 2 Typical Profiles observed at Uchinada Coast

Fig. 3 UAV used in this study (DJI Phantom 3 Professional quadcopter)

Figures 2 represent the typical profiles of the survey line located near the study area. The profiles were measured by Hokuriku Regional Development Bureau (hereafter referred to as HRDB), Ministry of Land, Infrastructure, Transport, and Tourism, Japan. The line of bathymetric survey was taken on the direction of 307 degrees clockwise from the North. This is slightly different from the normal direction to the local shoreline. The bed elevation is expressed with reference to Tokyo Peil (T.P.) datum, that is the standard Japanese datum of leveling based on the mean sea level of Tokyo Bay. Subaqueous profiles have been measured once a year by echo soundings. Hereafter, the cross-shore distance is computed with respect to the mean location of shoreline (defined as the location of 0 m T.P. elevation) during 1998 and 2010.

Existence of sandbars are recognized in the profiles until 2006. More recently, however, the magnitude of bars diminished. Relatively smooth profile is observed at 2010. Strong trend of accretion is observed over the whole area in Fig. 2. The mean profile during 1998 to 2010 is shown in Fig. 2(b). The average slope seaward from the mean shoreline is approximately 1/70, 1/200, 1/140 in the area 0~300 m, 300~500 m, 500~1300 m, respectively.

METOHDS OF ANALYSIS

The application of UAV in the monitoring of coastal morphological environments typically consists of the acquisition of high resolution images during UAV flight, and subsequent quantification of morphological changes based on image analysis.

Image acquisition from UAV

Recently, several platforms are available for airborne observation of sea surface. Among them we selected a commercially available UAV, DJI Phantom 3 Professional (P3P) quadcopter (Fig. 3), because of its high resolution imagery, excellent stability, and low cost. The use of quadcopter is preferred in this study because it can hover stably at an assigned location with a few meter positional accuracies. These features enable us to obtain high resolution photographic images of sea surface from favorable location in a cost-efficient way. The measurement system was composed of P3P with its remote controller, a tablet with application software, and Ground Control Points (GCPs). The control of P3P is easy since the camera view and altitude are simultaneously displayed on the tablet of the operator. The weight and diagonal size (excluding the propellers) of P3P is 1.22 kg and 0.35 m, respectively. It is equipped with a high-resolution video camera (GoPro Hero 3) mounted on a gimbal system that ensures a three-axis camera stabilization. The Video camera has a full resolution of 1920 × 1080 pixels and a maximum framing rate of 30Hz at full resolution. A fully charged battery can fly the P3P for up to approximately 20 min in mild weather (wind) conditions. Field observations were performed by flying the P3P at the Uchinada Coast on the day with mild wind condition. Video images were recorded for at least several minutes in each observation, during which sufficient numbers of wave images can be collected for bathymetry retrieval.

Ground control points are needed to conduct image rectification and adjustment. Since the surveyed area did not provide well defined points to be used as GCPs, it was decided to place artificial GCPs on the sandy beach surface. In the field observations, several sheets of contrasting colors (red sheets or blue sheets) were placed on the beach surface and fixed with pegs. The size of these sheets was approximately 1 m. The coordinates of these GCPs were measured by a handy GPS (Garmin eTrex). The video images were taken so that multiple GCPs were always included in the image. Figure 4 is an example of a snapshot taken from the P3P at an altitude of approximately 150 m, in which several GCPs (red sheets) are seen in the lower part of the picture.

Fig. 4 An example of snapshots obtained from the P3P

Image analysis

Adjustment of Images

Firstly, the video recorded movies were converted into a number of successive snapshots at a specified temporal interval. The lens distortion was then removed by using an image processing software (Adobe Photoshop). Although the UAV was operated in the hovering mode and the camera was stabilized by a high-performance gimbal equipped with P3P, it was occasionally suffered from small horizontal and vertical drift due to wind action. And therefore, the obtained images inevitably included small oscillations. The obtained images were therefore adjusted in order to minimize this kind of small oscillations based on the GCPs included in each picture. First, the locations of GCPs were semi-automatically identified for each frame individually. In each image, small search windows were set where the RGB information of individual pixel were inspected. Intensity thresholds were specified for the RGB values according to the color features of the sheets used for GCPs in the pictures. If the RGB values at a pixel satisfied the specified criteria, the pixel was judged to be within the GCP sheet. The center of mass within each GCP area was then computed. Based on the computed location of GCPs in each image, the spatial scaling was adjusted so that the size of a pixel was the same through all of the images. In addition, the images were rectified through rotation and translation so that the image coordinate in each picture would be the same.

Tracking of wave crests

The subsequent quantification of morphological changes was carried out based on bright intensity patterns. After removing the small oscillations through semi-automatic identification of GCPs, the color images were converted to grayscale format. Time series of pixel intensities were then sampled along a cross-shore transect for a series of images with a sampling interval Δt_s. The time-stack images, namely, the space-time imageries of bright intensity variations were constructed as shown in Fig. 5. The slightly curved patterns in the time-stack images represent individual wave crest propagating onshore.

Next, the lines of wave crest were tracked out by inspecting the location of steep gradient in bright intensity variations. First, a Laplacian filtering was applied in order to emphasize the location of steep gradients in the time-stack image. The temporal variation of bright intensity was then inspected at a series of discrete cross-shore positions (horizontal section $y=y_i$, i=1,2,3,…,n in Fig.5; hereafter called as inspection locations). In the temporal variation of brightness at $y=y_i$, in general, multiple points could be found where the bright intensity became maximal. Among these maximal points, only the points with their intensity greater than specified threshold were selected as the initial candidates representing wave crest. Here the threshold value was set as temporal average plus 1.5 times standard deviation at $y=y_i$. The time stack images often included high brightness points that were related to the foams remained after wave breaking. In order to remove the influence of these foams, the points that were close (less than ten time pixels in this study) to the prior candidate of wave crest were removed. Examples of the selected points describing the wave crest were shown as red markers in Fig. 5.

Estimation of Wave Celerity

After the selection of candidate points representing wave crest was completed, the crest line of propagating wave was constructed. Examples of traced wave crests are shown as blue lines in Fig. 5. Prior to the connection of individual crest line, expected range of local water depth was estimated at the inspection locations $y=y_i$ based on the typical foreshore slope observed at the study area and the seaward distance from the shoreline that was computed from the image. The crest lines were then traced by connecting successive candidate points obtained in the previous section. The procedure started from the most seaward location $y=y_1$. In general, there were multiple candidate points there, and the tracking started from the leftmost point ($P_{1,1}$). Here the first subscript is the index of individual crest line, and the second one represents the successive number of points. The next point to be connected was then searched at $y=y_2$. If a candidate point $P_{1,2}$ was found within the expected range of time interval inferred from the combination of expected range of local water depth, corresponding long-wave celerity, and the sampling interval, the crest line was connected from $P_{1,1}$ to $P_{1,2}$. If there is no suitable point on the next line, that crest line was disconnected. Similar procedures were repeated until whole of the time-stack image was covered.

In order to estimate the local wave celerity, the slope of the wave traces were computed. The estimation of celerity was conducted at specified cross-shore interval where the size of this interval was determined so that sufficient number of inspection lines was included in each

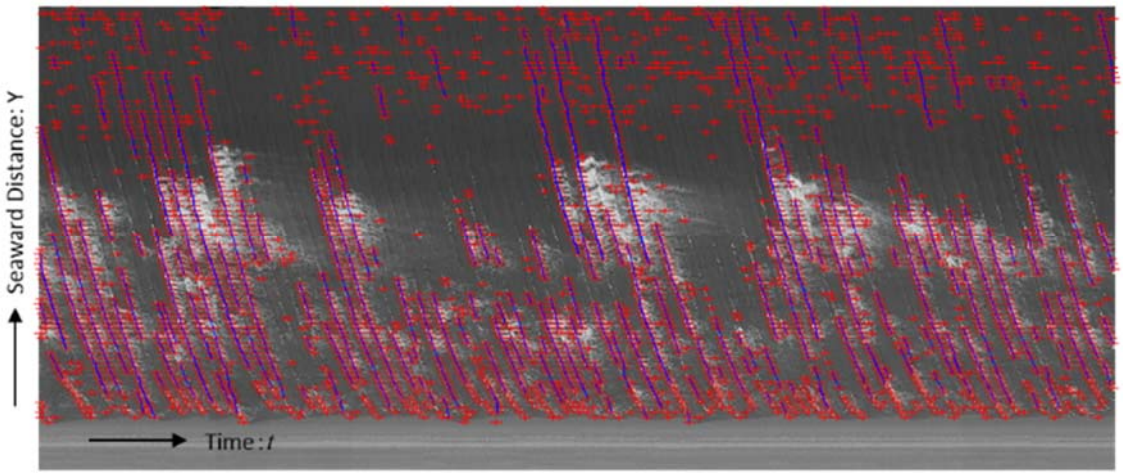

Fig. 5 An example of wave crest tracking in time-stack image. The horizontal and vertical direction correspond to time and seaward distance respectively. The red markers denote the candidate of wave crest and blue lines are the connected wave crest lines.

interval. The local slope of individual crest line was determined as the approximate celerity of the propagating waves based on least-square method for the points of individual crest line within each interval.

Estimation of Local Water Depth

Subsequently the linear dispersion relationship was applied to retrieve the corresponding local water depth. It is assumed that the bottom is mildly sloping as:

$$O(\nabla h/kh) \ll 1 \tag{1}$$

in which h is the local water depth and the wave number k is defined as $2\pi/(CT)$ with T the wave period. It is also assumed that the incoming wave directions are nearly normal to the shoreline. The linear dispersion relation then relates the wave number and frequency through

$$\sigma^2 = gk \tanh(kh) \tag{2}$$

where angular frequency σ is defined as $2\pi/T$, and g the gravity acceleration. Accordingly, if the wave celerity and wave period are known, the water depth can be estimated from equation (2) as follows:

$$h = \frac{2\pi}{cT} gk \tanh^{-1}\left(\frac{2\pi C}{gT}\right) \tag{3}$$

At the limit of shallow water, it can be simplified as:

$$h = \frac{C^2}{g} \tag{4}$$

Combined with the mean wave period observed at Kanazawa Port by the NOWPHAS measurement system, the local water depth was estimated based on the equations (3) and (4). In general, multiple lines of different wave crests were included in a time-stack image, and different estimate was obtained for each wave at the same cross-shore location. The median value of the estimates was selected as the local water depth there.

The water depth inversion described above was carried out for a series of cross-shore sections located at specified alongshore intervals. The tidal correction was then conducted according to the tidal record at Kanazawa Port. The synthesis of the results for multiple transects finally provided the bathymetry mapped in the horizontally two-dimensional field.

Bathymetric Survey

The bathymetric survey was conducted in the afternoon of Oct./05/2015 by HRDB. During the field survey, the significant wave height was around 0.75 m, and the wave period was around 5.7 s, according to the wave record observed at Kanazawa Port. The principal incoming wave direction was from the WNW or the NW. The tide level was 0.20 m (T.P.). The bathymetry was measured along a number of alongshore transects extending approximately 1 km using a jet-bike. The cross-shore interval between successive lines of survey was approximately ten meters. In the cross-shore direction, the survey area covered the area approximately 100 to 250 m range from the shoreline. A mobile measurement device (RiverSurveyorM9) was mounted on the jet-bike. The position of the jet-bike was recorded based on a GPS system. In the surveyed area, equidistant grid points with specified interval in cross-shore and alongshore directions were constructed. The local water depth at each grid point was determined as the median of the observed depth collected in the neighborhood of that point.

The corresponding image-based observation was conducted by HRDB on Sep./29/2015. During the UAV observation, the significant wave height was around 1.0 to 1.3 m, and the wave period was around 5.8 to 6.5 s, according to the wave record observed at Kanazawa Port.

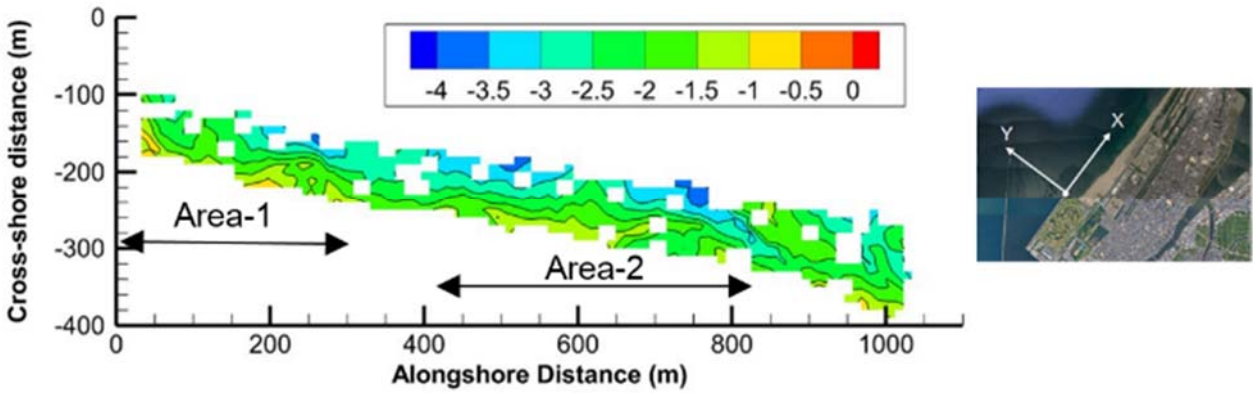

Fig. 6 Bathymetry obtained by the jet-bike survey on Oct./05/2015. The origin is located on the south-east end of the eastern groin of Kanazawa Port. The vertical direction is 306 degrees clockwise from the North, and is parallel to the eastern groin of Kanazawa Port.

The video monitoring was performed for several subareas that covered the surveyed area as a whole. During the survey the weather was sunny with low wind conditions (5 to 7 m/s). Video images were recorded for seven to ten minutes for each observation. The UAV was always set to view vertically downward. The hovering height of the UAV was set to comply with 150-m maximum height according to the regulations in Japan.

It is noted that the bathymetric survey was conducted six days after the UAV measurement. During this period approximately 4 m of significant wave height was observed on Oct./02/2015. The bathymetry may have been influenced by this event.

Verification of applicability

As an initial validation of the stability and accuracy of image processing, the remained oscillations in the GCP locations in the adjusted images were inspected. The centroids of extracted GCPs were computed and compared among a series of images.

Next, the spatial variation of water depth at the study area was examined based on the bathymetric survey. The image-based estimation of bathymetry was then compared with field survey. The reproducibility of two-dimensional spatial variation pattern as well as the bed profiles on the cross-shore and alongshore transects were investigated. The characteristics of estimation error was examined for the proposed system.

RESULTS AND DISCUSSIONS

Stability of UAV measurements and image processing

If the adjustments of images were exactly conducted without error, the locations of GCPs would be completely identical among all of the images. In the real observation, however, the locations of GCPs suffer from small oscillation due to several kinds of errors even after the adjustment operations. Accordingly, the accuracy of image adjustments was examined quantitatively. The standard deviation of the pixel location of the centroid of each GCPs were computed for the same series of images. Typically, the standard deviation of the fluctuation in centroid locations of GCPs in pixel coordinate was found to be around 0.5 to 1.5 pixel. This is in the same order of image resolution. Accordingly, the UAV-based image acquisition and subsequent image processing provided reliable basis for retrieving nearshore bathymetry.

Characteristics of observed bathymetry

The bathymetry obtained from the field survey is shown in Fig. 6. The water depth within the survey area was generally in the range 0.8 to 4.0 m. The survey could not cover the area where the depth was less than approximately 1 m. The blank area in the plot indicates that the obtained data were not enough for bathymetry computation at that location. The contour lines of bed level was generally parallel to the shoreline, while moderate modulation was seen in several places. The contour line protruded near the eastern groin of Kanazawa Port. The error of measurement induced by the wave-induced jet-bike motion is considered to be ±0.10 to 0.40 m. This is much larger than that of the depth measurement device itself. The error in horizontal location in GPS measurements is estimated to be several meters.

Comparison with Bathymetric Survey

The bathymetry estimated from the image analysis was compared with field survey. The results of comparison are shown for the two sub-areas indicated in Fig. 6. The Area-1 is located on the left end of the surveyed area and is close to the eastern groin of Kanazawa Port. The Area-2 is located in the middle of the surveyed area. Figure 7 indicates the time-averaged image of these sub areas. The formation of shoals are recognized

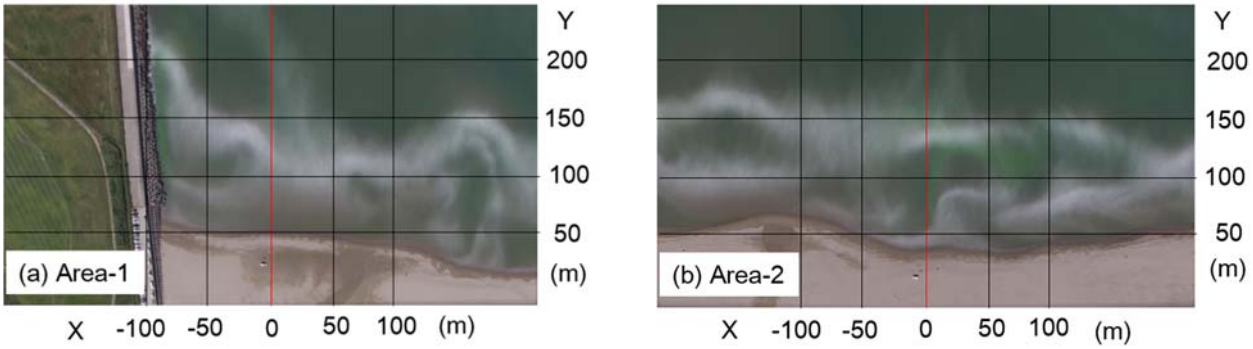

Fig. 7 Time-averaged image

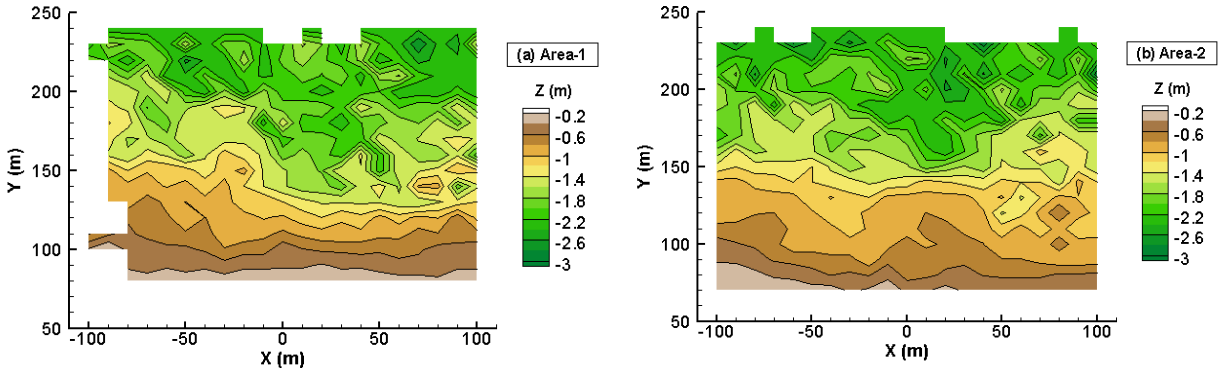

Fig. 8 Horizontally two-dimensional bathymetry estimated from image analysis

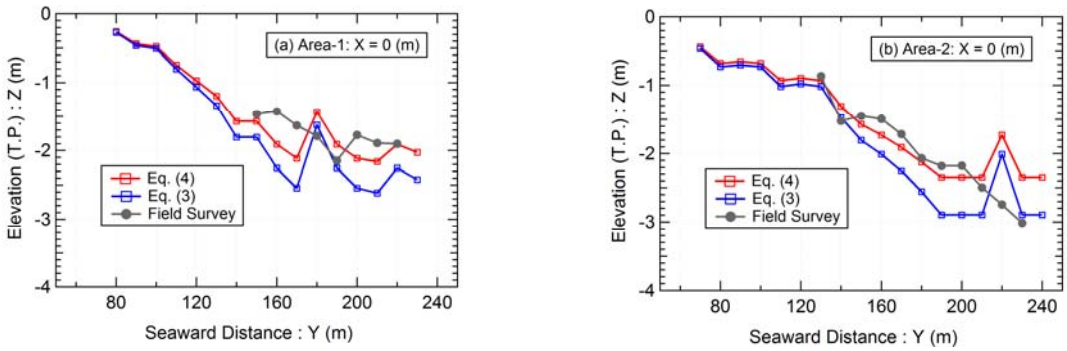

Fig. 9 Comparison of retrieved profile and surveyed profile on a cross-shore transect

as white bands where the wave breaking was intensified. The estimated bathymetry in the sub-areas are plotted in Figs. 8. These figures were made based on long-wave assumption, namely equation (4). The estimated range of depth was mainly in the range 0.5 to 3 m and roughly coincided with the field survey. In Fig. 6, the field survey demonstrated that the contour lines is advanced near the groin, and this feature was well reproduced in the image-based depth estimation in Fig. 8(a). Comparison between the time averaged image and retrieved bathymetry indicated that the location of the white bands are close to the line of 1.2 m depth. It seemed that the breaker depth during the image acquisition was around 1.2 m. The image-based estimation of bathymetry provided qualitatively good results.

Figure 9 show the examples of comparison of profiles in the cross-shore directions. The locations of these transects were taken at the center of Fig. 7(X= 0 m). The results based on equations (3) and (4) were compared with field survey. The results demonstrated that the agreements between the image analysis and jet-bike survey was satisfactory until seaward distance is around 190 m where the water depth reached around 2.5 m. The image-based estimation reproduced the general features of the profiles there. The results derived from long-wave assumption provided better estimation in these cases. On the contrary, in the area where Y > 200 m, larger estimation error of around 0.8m was seen at some locations. It is noted that in the area where wave breaking are scarcely observed, the tracking of wave crest may become erroneous, because the intensity variation was not significant and only small number of waves can be identified. Similarly,

image-based profiles on alongshore transects were compared with bathymetric survey. The results also indicated that the accuracy of bathymetry retrieval was satisfactory on the transects located relatively close to the shoreline (relatively shallow depth), while the estimation error was enlarged at the transects located more seaward.

In addition to the failures in the extraction of crest lines at offshore area, several other causes are considered to be related with the estimation error in image-based analysis. Both of the field survey and image analysis may have a positioning error up to a couple of meters. The relatively high waves on Oct./2/2015 possibly influenced the bathymetry. In future study, the influence of oblique incidence of waves and the irregularity of wave period should be incorporated.

SUMMARY REMARKS

In this study, a local remote sensing system was developed in order to monitor morphological variations of sandy beaches. This monitoring system consists of acquisition of geo-referenced video image of nearshore area from a small UAV and subsequent image analysis. The UAV selected for use in this study was DJI Phantom-3. The subsequent quantification of morphological changes was carried out based on bright intensity patterns. First, the video images were converted to successive snapshots and rectified. The lens distortions and small oscillations were then removed semi-automatically. The crest lines of waves were tracked out by inspecting the location of steep gradient in bright intensity variations in the time-stack images for a series of cross-shore sections. The local tracking results provided the local celerity of waves. With the help of linear wave theory, the local water depth was estimated based on the dispersion relation. Finally, the synthesis of the estimated results on a set of transects located at specified alongshore intervals provided a horizontally two-dimensional variation of the nearshore bathymetry.

The system was applied to the field observation of Uchinada Coast, Ishikawa, Japan facing to the Sea of Japan. The accuracy of geo-referencing was shown to be as small as a couple of pixels. The accuracy of morphological estimation based on image processing has been confirmed through a comparison with a field survey using a jet bike. The image-based estimation results qualitatively reproduced the patterns of morphological variation. The typical error was in the range 0.2 to 0.8 m. These results demonstrated the high capability of the developed system to remotely measure the coastal morphology on sandy beaches.

ACKNOWLEDGEMENTS

The records of field survey were provided by HRDB. The wave data was obtained from the Japanese NOWPHAS dataset. This study was partially supported by Grants-in-Aid for Scientific Research by the Japan Society for the Promotion of Science (Nos. 16K06505 and 19H02244). Assistance rendered by Mr. Sasaki and Mr. Sogawa (former students of Kanazawa University) is acknowledged.

REFERENCES

Holman, R.A. and Stanley, J. (2007). The history and technical capabilities of Argus. Coastal Engineering, 54: 477-491.

Holman, R.A. and Haller, M.C. (2013). Remote Sensing of the Nearshore. Annual Review of Marine Science. 5: 95-113.

Holman, R.A., Brodie, K.L., and Spore, N.J. (2017). Surf Zone Characterization Using a Small Quadcopter: Technical Issues and Procedures, *IEEE Transactions on Geoscience and Remote Sensing*, 55(4): 2017- 2027

Kuroiwa, M., Sueyoshi, R., Ichimura, Y., and Fukuoka, K., S. (2016). Study on Coastal Topographic Change Analysis Utilizing UAV. *Journal of Japan Society of Civil Engineers. Ser. B*3 (*Ocean Engineering*), 72(2): I_784–I_789 (in Japanese).

Matsuba, Y. and Sato, S., (2018). Nearshore bathymetry estimation using UAV, *Coastal Engineering Journal*, 60(1): 51-59.

Nagai, T. Sugahara, K., Hashimoto, N., Asai, T., Higashiyma, S., and Toda, K., (1994): Introduction of Japanese NOWPHAS system and its recent topics, *Proc. Int. Conf. on Hydro-Technical Eng. for Port and Harbor Construction* (*HYDRO-PORT*'94), *PHRI*, 67-82.

Nguyen, T.C. and Yuhi, M., (2015): Long-term variation of wave characteristics on the Kaetsu Coast, Japan, *Journal of Japan Society of Civil Engineers*, *Ser. B*3 (*Ocean Engineering*), 71(2), I_359-I_364.

Sun, S.H., Chuang, W.L., Chang, K.A., Kim, J.Y., Kaihatu, J., Huff, T., and Feagin, R. (2019). Imaging-based nearshore bathymetry measurement using an unmanned aircraft system. *Journal of Waterway, Port, Coastal, and Ocean Enigneering, ASCE*. 145(2): 04019002.

Wright, L. D. and Short, A. D. (1984). Morphodynamic variability of surf zones and beaches: a synthesis. *Marine Geology*, 56, 93-118.